Inhibition of organic cation transporter (OCT) activities by carcinogenic heterocyclic aromatic amines

Katia Sayyed, Christophe Camillerapp, Marc Le Vée, Arnaud Bruyère, Anne T Nies, Ziad Abdel-Razzak, Olivier Fardel

Inhibition of organic cation transporter (OCT) activities by carcinogenic heterocyclic aromatic amines

Katia Sayyed[1,2], Christophe Camillerapp[1], Marc Le Vée[1], Arnaud Bruyère[1], Anne T. Nies[3], Ziad Abdel-Razzak[2], Olivier Fardel[1,4,*]

[1] Univ Rennes, Inserm, EHESP, Irset (Institut de recherche en santé, environnement et travail) - UMR_S 1085, 2 Avenue du Pr Léon Bernard, 35043 Rennes, France

[2] EDST-AZM-center-LBA3B, Faculty of Sciences, Rafic Hariri Campus, Lebanese University, Lebanon

[3] Dr. Margarete Fischer-Bosch Institute of Clinical Pharmacology, Stuttgart and University of Tübingen, Auerbachstrasse 112, 70376 Stuttgart, Germany

[4] Pôle Biologie, Centre Hospitalier Universitaire, 2 rue Henri Le Guilloux, 35033 Rennes, France

* Corresponding author at : Irset (Institut de recherche en santé, environnement et travail) - UMR_S 1085, Faculté de Pharmacie, 2 Avenue du Pr Léon Bernard, 35043 Rennes, France

Abstract

Carcinogenic heterocyclic aromatic amines (HAAs) interact with some drug transporters, like the efflux pump BCRP and the organic anion transporters OAT1 and OAT3. The present study was designed to determine whether they can also target activities of the organic cation transporters (OCTs), using mainly OCT1-, OCT2- and OCT3-overexpressing HEK293 cells. Fifteen HAAs were demonstrated to differently alter OCT activities; with a cut-off of at least 50% reduction of transporter activity by 100 µM HAAs, 5/15 HAAs, including Trp-P-1 and Trp-P-2, inhibited activities of OCT1, OCT2 and OCT3, whereas 7/15 HAAs, including PhIP and MeIQx, blocked those of OCT2 and OCT3, 1/15 HAAs reduced those of OCT1 and OCT2 and 2/15 HAAs, including AαC, only that of OCT2. IC_{50} values of Trp-P-1 and Trp-P-2 towards OCT activities were found to be in the 2-6 µM range, likely not relevant for human exposure to HAAs through smoking or the diet. Trp-P-1 and Trp-P-2 additionally failed to *trans*-stimulate OCT1 and OCT2 activities and exhibited similar accumulation in OCT1/2-transduced HEK293 cells and control HEK293-MOCK cells. These data demonstrate that HAAs, notably Trp-P-1 and Trp-P-2, interact with OCT1/2, without however being transported, thus likely discarding a major role for OCT1/2 in HAA systemic toxicokinetics.

Key-words: Drug transporter; toxicokinetics; organic cation transporter; heterocyclic amines; toxicity.

1. Introduction

Heterocyclic aromatic amines (HAAs) are chemicals containing at least one heterocyclic ring, as well as at least one amine (nitrogen-containing) group; typically, it is a nitrogen atom of an amine group that also makes the ring heterocyclic. Various HAAs can be found in cooked meat and cigarette smoke and exert mutagenic and carcinogenic effects for most of them (Sugimura et al., 2004; Talhout et al., 2011; Turesky and Le Marchand, 2011). Such HAAs belong to two main classes: pyrolytic/aminocarbolins and thermic/aminoimidazoarenes (Cheng et al., 2006). Pyrolytic HAAs come from high-temperature (>250°C)-related pyrolysis of proteins or amino acids and notably comprise 2-amino-9H-pyrido[2,3-b]indole (AαC), the major carcinogenic HAA found in tobacco smoke (Zhang et al., 2011), 2-amino-3-methyl-9H-pyrido[2,3-b]indole (MeAαC), 2-amino-6-methyl[1,2-a:3',2''-d]imidazole (Glu-P-1), 2-aminodipyrido[1,2-a:3',2''-d]imidazole (Glu-P-2), 3-amino-1,4-dimethyl-5H-pyrido [4,3-b]indole (Trp-P-1), 3-amino-1-methyl-5H-pyrido[4,3-b]-indole (Trp-P-2) and the non-mutagenic β-carbolins methyl-9H-pyrido[3,4-b]indole (Harmane) and 9H-pyrido[3,4-b]indole (Norharmane). Thermic/aminoimidazoarenes HAAs such as 2-amino-1-methyl-6-phenylimidazo(4,5-b)pyridine (PhIP) and 2-amino-3-methyl-imidazo [4, 5-f] quinoline (IQ) are formed at lower temperature (150-250°C) than pyrolytic HAAs, through notably the Maillard reaction between hexoses and amino acids during meat cooking (Turesky, 2007).

To be mutagenic or carcinogenic, dietary and environmental HAAs require metabolic activation (Turesky, 2002). In humans, this occurs primarily in the liver through the phase I enzyme cytochrome P-450 (CYP) 1A2-mediated N-oxidation of the exocyclic amine groups of HAAs, to form N-hydroxy-HAA derivatives (Langouet et al., 2001). In extrahepatic tissues, CYP1A1 and CYP1B1 contribute also to the bioactivation of HAAs (Shimada et al., 1996).

Subsequent acetylation or sulfation of N-hydroxy-HAAs by some phase II drug metabolizing enzymes like N-acetyl-transferase or sulfo-transferase produces highly unstable esters, which react with DNA to form mutagenic adducts, through notably the formation of arylnitrenium ions (Turesky and Le Marchand, 2011). These reactive species can however be detoxified by glutathione -*S*-transferases (Coles et al., 2001), whereas other phase II conjugating enzymes such as UDP-glucuronosyl-transferases directly inactivate N-hydroxy-HAAs (Stillwell et al., 1999).

In addition to drug metabolizing enzymes, ATP-binding cassette (ABC) drug transporters can participate to disposition and detoxification of HAAs. Indeed, PhIP and its metabolites are eliminated *in vivo* by the ABC efflux pumps P-glycoprotein (P-gp/*ABCB1*), encoded by the multidrug resistance gene 1 (*MDR1*), multidrug resistance-associated protein 2 (MRP2/*ABCC2*), and breast cancer resistance protein (BCRP/*ABCG2*) (van Herwaarden et al., 2003; Walle and Walle, 1999). BCRP also handles Trp-P-1 and IQ (van Herwaarden et al., 2006). Because ABC transporters are notably localized at the apical domain of enterocytes and at the canalicular domain of hepatocytes, they likely reduce systemic exposure to HAAs by preventing their intestinal absorption and by contributing to their biliary elimination (Dietrich et al., 2001; Vlaming et al., 2014). Besides ABC efflux pumps, solute carrier (SLC) transporters, which mainly mediate drug uptake into cells through facilitated diffusion or secondary active transport (Giacomini et al., 2010), are presumed to also interact with HAAs. Indeed, PhIP and AαC have been shown to block activities of the renal organic anion transporter (OAT) 3 (*SLC22A8*), without probably being handled by this transporter (Sayyed et al., 2017); OAT3 activity is also inhibited by Trp-P-2, whereas PhIP blocks that of OAT1 (*SLC22A6*). Trp-P-1 and Trp-P-2 have additionally been postulated to be transported by the dopamine active transporter (DAT/*SLC6A3*) and the serotonin transporter (SERT/*SLC6A4*) (Hashimoto et al., 2002; Naoi et al., 1989). Whether HAAs may

interact with other SLC drug transporters remains unknown, but is probably important to determine, owing to the now well-established role of SLC transporters in xenobiotic disposition (Zhou et al., 2017). In this context, it is likely important to consider the putative interactions of HAAs with organic cation transporters (OCTs) (Jonker and Schinkel, 2004), such as OCT1 (*SLC22A1*) and OCT2 (*SLC22A2*), expressed mainly at the basolateral pole of hepatocytes and proximal tubular cells, respectively, and OCT3 (*SLC22A3*), found in various tissues and organs. Indeed, such transporters handle various amine drugs and biogenic amines (Nies et al., 2011b), thus suggesting that they may interact with additional amines such as HAAs. The fact that dopamine, a physiological amine substrate for OCT1 and OCT2 (Grundemann et al., 1999), can inhibit cellular uptake of Trp-P-1 and Trp-P-2 (Hashimoto et al., 2002) likely supports this hypothesis. The present study was therefore designed to determine whether HAAs may interact with OCTs using mainly OCT1-, OCT2- and OCT3-overexpressing cells. Our data demonstrate that various HAAs can inhibit activities of OCTs. It is notably the case for the pyrolytic HAAs Trp-P-1 and Trp-P-2, which inhibit activities of OCT1, OCT2 and OCT3, without however being transported by OCT1 and OCT2, thus making unlikely a contribution of these SLC transporters to their toxicokinetics.

2. **Materials and methods**

2.1 Chemicals

HAAs were provided by Santa Cruz Biotechnology (Dallas, TX, USA). They correspond to eight pyrolytic/aminocarbolin HAAs, *i.e.*, AαC, MeAαC, Trp-P-1, Trp-P-2, Glu-P-1, Glu-P-2, harmane, and norharmane, and seven thermic/aminoimidazoarenes HAAs, *i.e.*, PhIP, IQ, 2-amino-3-méthyl-3H-imidazo[4,5-f]quinoxaline (IQx), 2-amino-3,4-dimethyl-3H imidazo[4,5-f]quinoline (MeIQ), 2-amino-3,8-dimethylimidazo[4,5-f]quinoxaline (MeIQx), 2-amino-3,4,8-

trimethylimidazo[4,5-f]quinoxaline (4,8-diMeIQx) and 2-amino-3,7,8 trimethylimidazo[4,5-f]quinoxaline (7,8-diMeIQx). These fifteen HAAs are listed in Table 1 and their chemical structures are indicated in Figure 1. Amitriptyline, verapamil, cyclosporine A, fumitremorgin, bromosulfophthalein (BSP), tetraethylammonium bromide (TEA), corticosterone and 3-(4,5-dimethylthiazol-2-yl)-2,5-diphenyltetrazolium bromide (MTT) were provided by Sigma-Aldrich (Saint-Quentin Fallavier, France), whereas carboxy-2.7- dichlorofluorescein (DCF) and Hoechst 33342 were from Life Technologies (Villebon sur Yvette, France) and 4 (4-(4-(dimethylamino)styryl) -N-methylpyridinium iodide (ASP^+) from Thermo Fisher Scientific Inc. (Waltham, MA, USA). [1-^{14}C] TEA (specific activity = 3.5 mCi/mmol) was from Perkin-Elmer (Boston, MA, USA). All other chemicals and reagents were commercial products of the highest purity available.

2.2 Cell culture

HEK293 cells overexpressing OCT1 (HEK-OCT1 cells), OCT2 (HEK-OCT2 cells), MATE (Multidrug and toxin extrusion transporter) 1 (*SLC47A1*) (HEK-MATE1 cells), MATE2-K (*SLC47A2*) (HEK-MATE2-K cells) or OATP (organic anion transporting polypeptide) 1B1 (*SLCO1B1*) (HEK-OATP1B1 cells), as well as control HEK-MOCK cells were prepared by transduction of HEK293 cells by lentiviral vectors containing the respective human cDNA of the transporters (HEK-transporter cells) or by empty lentiviral vector (HEK-MOCK cells), as previously described (Jouan et al., 2014). HEK293 cells overexpressing OCT3 (HEK-OCT3 cells) were obtained by transfection of an expression vector containing human cDNAs encoding the OCT3 transporter and a G418 resistance marker (Nies et al., 2011a); HEK-control cells (HEK-CTR cells) were obtained in parallel by transfection of a vector containing only the G418 resistance marker. Transduced and transfected HEK293 cells were cultured in Dulbecco's modified Eagle

medium (DMEM) (Life Technologies), supplemented with 10% (vol/vol) fetal calf serum, 10 IU/mL penicillin, 10 µg/mL streptomycin, 1% nonessential amino acids, and 1 µg/mL insulin. G418 (800 µg/mL) was added for the culture of HEK-OCT3 and HEK-CTR cells, as a selection agent. HEK293 cells overexpressing BCRP (HEK-BCRP cells) (Tournier et al., 2010), kindly donated by Dr X. Decleves (Faculty of Pharmacy, University Paris-Descartes, Paris, France), were cultured in DMEM, supplemented with 10% (vol/vol) fetal calf serum, 100 IU/mL amoxicillin, 100 µg/mL erythromycin and 2 mg/mL G418. P-gp-overexpressing mammary MCF7R cells (Jouan et al., 2016) were cultured in DMEM, supplemented with 10 % (vol/vol) fetal calf serum, 10 IU/mL penicillin and 10 µg/mL streptomycin.

Human highly-differentiated hepatoma HepaRG cells, which constitutively express OCT1 (Le Vee et al., 2013), were cultured in Williams' E medium (Life Technologies) supplemented with 10% (vol/vol) fetal calf serum, 10 IU/mL penicillin, 10 µg/mL streptomycin, 5 µg/mL insulin, 2 mM glutamine, and 5 x 10^{-5} M hydrocortisone hemisuccinate. Additional culture for two weeks in the same medium supplemented with 2% (vol/vol) dimethylsulfoxide was performed in order to get a full hepatocytic differentiation of the cells (Gripon et al., 2002).

2.3 SLC transporter activity assays

SLC transporter activities were analyzed through determining intracellular accumulation of reference fluorescent or radiolabeled substrates of these SLC transporters at 37°C for 5 min (SLC transporter-overexpressing HEK293 cells) or 10 min (HepaRG cells), in the absence or presence of reference inhibitors or tested HAAs, as previously described (Chedik et al., 2017; Le Vee et al., 2015; Sayyed et al., 2017). The reference substrates were 10 µM ASP^+ (for OCTs), 28.6 µM [1-^{14}C] TEA (for OCT1 and MATEs) and 10 µM DCF (for OATP1B1). The reference inhibitors were amitriptyline (100 and 200 µM for OCT2 and OCT1, respectively), 100 µM corticosterone (for

OCT3), verapamil (50 and 200 µM for OCT1 and MATEs, respectively) and 100 µM BSP (for OATP1B1). The transport assay medium consisted of 5.3 mM KCl, 1.1 mM KH_2PO_4, 0.8 mM $MgSO_4$, 1.8 mM $CaCl_2$, 11 mM D-glucose, 10 mM HEPES, and 136 mM NaCl; pH was adjusted to 7.4 value, except for the pH-sensitive MATE1 and MATE2-K transport assay for which pH was set at 8.4 (Chedik et al., 2017). After incubation with substrates and subsequent washing with phosphate-buffered saline (PBS), cells were lysed in distilled water. Intracellular accumulation of radiolabeled substrates was next measured by scintillation counting, whereas intracellular accumulation of ASP^+ and DCF was determined by spectrofluorimetry using a SpectraMax Gemini SX spectrofluorometer (Molecular Devices, Sunnyvale, CA, USA); excitation and emission wavelengths were 492 and 517 nm, respectively, for DCF, and 485 nm and 607 nm respectively, for ASP^+. Values of substrate accumulation were then normalized to total protein content, determined by the Bradford method (Bradford, 1976). Data were finally expressed as percentages of transporter activity found in control cells not exposed to inhibitors or HAAs, arbitrarily set at 100%, according to the following equation:

$$(\%)\ \text{SLC transporter activity} = \frac{(\text{Accumulation}_{\text{HAA}} - \text{Accumulation}_{\text{Reference inhibitor}})}{(\text{Accumulation}_{\text{Control}} - \text{Accumulation}_{\text{Reference inhibitor}})} \times 100 \qquad (A)$$

with $\text{Accumulation}_{\text{HAA}}$ = substrate accumulation in the presence of HAA, $\text{Accumulation}_{\text{Reference inhibitor}}$ = substrate accumulation in the presence of the reference inhibitor and $\text{Accumulation}_{\text{Control}}$ = substrate accumulation in untreated cells.

Percentages of OCT activity inhibition in the presence of HAAs were calculated according to the following equation:

$$(\%)\ \text{OCT activity inhibition} = 100\% - (\%)\ \text{OCT transporter activity}_{\text{HAA}} \qquad (B)$$

with $(\%)\ \text{OCT transporter activity}_{\text{HAA}}$ = OCT transporter activity in the presence of HAA, determined as described in equation (A).

2.4 ABC transporter activity assays

ABC transporter activities were analyzed through measuring intracellular accumulation (for P-gp) or retention (for BCRP) of fluorescent substrates, in the absence or presence of reference inhibitors or HAAs, as previously described (Fardel et al., 2015; Le Vee et al., 2015).

For P-gp activity, P-gp-expressing MCF7R cells were incubated with 5.25 µM rhodamine 123 for 30 min at 37°C, in the presence or absence of 100 µM cyclosporine A or HAAs. After washing with PBS, cells were lysed and intracellular accumulation of the fluorescent dye was next determined by spectrofluorimetry (excitation and emission wavelengths were 485 and 535 nm, respectively). Data were normalized to total protein content and expressed as percentages of transporter activity found in control cells, arbitrarily set at 100%, according to the following equation:

$$(\%)\ \text{P-gp activity} = \frac{(\text{Accumulation}_{\text{CSA}} - \text{Accumulation}_{\text{HAA}})}{(\text{Accumulation}_{\text{CSA}} - \text{Accumulation}_{\text{Control}})} \times 100 \qquad (C)$$

with $\text{Accumulation}_{\text{HAA}}$ = substrate accumulation in the presence of HAA, $\text{Accumulation}_{\text{Control}}$ = substrate accumulation in control cells and $\text{Accumulation}_{\text{CSA}}$ = substrate accumulation in the presence of the reference P-gp inhibitor cyclosporine A.

For BCRP activity, HEK-BCRP cells were first loaded at 37°C with 16.2 µM Hoechst 33342 for 30 min. After washing in PBS, cells were re-incubated in Hoechst 33342-free medium at 37°C for 90 min in the absence or presence of 10 µM fumitremorgin C or HAAs. After washing in PBS, cells were lysed and intracellular retention of Hoechst 33342 was next determined by spectrofluorimetry (excitation and emission wavelengths were 355 and 460 nm, respectively). Data were normalized to total protein content and expressed as percentages of transporter activity found in control cells, arbitrarily set at 100%, according to the following equation:

$$(\%)\ \text{BCRP activity} = \frac{(\text{Retention}_{FTC} - \text{Retention}_{HAA})}{(\text{Retention}_{FTC} - \text{Retention}_{Control})} \times 100 \qquad (D)$$

with Retention_{HAA} = substrate retention in the presence of HAA, $\text{Retention}_{Control}$ = substrate retention in control cells and Retention_{FTC} = substrate retention in the presence of the reference BCRP inhibitor fumitremorgin C.

2.5 Determination of kinetic parameters

Kinetic parameters (V_{max}, K_m) of OCT1-, OCT2- and OCT3-mediated uptake of ASP^+ in HEK-OCT1, -OCT2 and -OCT3 cells were estimated using GraphPad Prism 5.0 software (GraphPad Software, La Jolla, CA, USA) by nonlinear regression based on the following Michaelis-Menten equation:

$$v = \frac{V_{max} \times [S]}{K_m + [S]} \qquad (E)$$

with ν is the initial transport rate of ASP^+ in HEK-OCT cells, [S] is the ASP^+ substrate concentration in the medium, K_m is the Michaelis-Menten affinity constant, and V_{max} is the maximum transport rate.

Half maximal inhibitory concentrations (IC_{50}) of HAAs towards OCT1, OCT2 or OCT3 activities, were determined from nonlinear regression of concentration-response data based on the four parameter logistic function. They were calculated using GraphPad Prism software through the following equation:

$$A = \frac{100}{1 + 10^{((([I] - \text{Log } IC_{50}) \times \text{Hill slope})}} \qquad (F)$$

with A is the percentage of transporter activity for a given concentration of HAA determined as described in equation (A), [I] is the HAA concentration in the medium, and Hill slope is a coefficient describing the steepness of the curve.

2.6 Trans-stimulation assays

Trans-stimulation assays were performed in HEK-OCT1 and HEK-OCT2 cells using the OCT1/OCT2 substrate TEA (Zhang et al., 1999). Briefly, HEK-OCT1 and HEK-OCT2 cells were first incubated with 2 mM unlabeled TEA or 100 µM of tested HAAs for 60 min at 37°C. After washing with PBS, cells were next re-incubated with radiolabeled [1-^{14}C]-TEA (used at 28.6 µM) for 5 min at 37°C. Intracellular accumulation of the radiolabeled TEA was finally determined as reported above. Data were expressed as percentages of [^{14}C]-TEA accumulation found in control cells not pre-treated by unlabeled TEA or HAAs.

2.7 Cell viability assay

Cell viability was assessed using a MTT colorimetric assay (Carmichael et al., 1987). Confluent HEK-OCT1, HEK-OCT2 or HEK-MOCK cells were either untreated (control) or treated with a range of concentrations (from 0.3 to 300 µM) of Trp-P-1 or Trp-P-2 for 24 h at 37°C. Cells were next incubated with 0.5 mg/mL MTT for 2 h, allowing the reduction of MTT into formazan dye by living cells (Mosmann, 1983). Formation of formazan dye, beforehand solubilized in dimethylsulfoxide, was next quantified by its absorbance at 540 nm using the spectrophotometer SPECTROstar nano (BMG Labtech, Ortenberg, Germany). Data for HAA-exposed cells were finally expressed as percentage of viability comparatively to untreated control cells, using the following equation:

$$(\%)\ \text{Cell viability} = \frac{\text{Absorbance}_{\text{HAA}}}{\text{Absorbance}_{\text{Control}}} \times 100 \qquad \text{(G)}$$

with Absorbance $_{HAA}$= aborbance of HAA-treated cells and Absorbance $_{Control}$ = absorbance of untreated control cells.

IC_{50} values of HAAs towards cell viability were determined using the equation (F), with A corresponding to the percentage of viability for a given concentration of HAA determined by the equation (G).

2.8 HAA accumulation quantification

HEK-OCT1, HEK-OCT2 and HEK-MOCK cells were incubated with 1 µM Trp-P-1 or 1 µM Trp-P-2, for 10 min at 37°C in the transport assay medium defined above. Cells were next washed twice with ice-cold PBS, and lysed in distilled water. An acetonitrile-based extraction of cell lysates was further performed, following by HAA quantification through liquid chromatography-tandem mass spectroscopy (LC-MS/MS), using an high-performance liquid chromatography Aria system (Agilent, Les Ulis, France), equipped with a Poroshell® C18 (4.6 x 150 mm) column (Interchim, Montluçon, France) and coupled to a tandem mass spectrometry TSQ Quantum Ultra (Thermo Fisher Scientific) fitted with an electrospray ionization source (ESI^+). Monitored ion transitions were at 212.1>167.1 m/z and 198.1>154.1 m/z for Trp-P-1 and Trp-P-2, respectively. Amounts of HAAs were finally normalized to total protein cell content.

2.9. Molecular descriptor generation

236 molecular descriptors belonging to the blocks “constitutional indices” (n=47), “functional group counts” (n=154), “charge descriptors” (n=15) and “molecular properties” (n=20), were determined using the Dragon 7.0 software (Talete, Milano, Italy) (See http://www.talete.mi.it/products/dragon_molecular_descriptor_list.pdf for a complete list of these descriptors). HAAs, initially expressed in SMILES format, were converted to 3D format using the MarvinView software (ChemAxon, Budapest, Hungary) before processing by Dragon 7.0 software to obtain molecular descriptors, as previously described (Chedik et al., 2017). An additional charge

descriptor, *i.e.*, the percentage of cationic form of HAAs at pH=7.4, was determined using Chemicalize software (ChemAxon).

2.9 Statistical analysis

Data were usually expressed as means ± SEM from at least three independent experiments, each being performed in triplicate. They were statistically analyzed using GraphPad Prism software through analysis of variance (ANOVA) followed by Dunnett's post-hoc test, Students'*t*-test or F-test. Correlation between molecular descriptor indexes and percentages of OCT activity inhibition by HAAs was done through Pearson correlation, after confirmation of normality of data distribution by D'Agostino and Pearson omnibus normality test. The criterion of significance for statistical tests was $p < 0.05$.

3. Results

3.1 Inhibition of OCT activities by HAAs

The effects of HAAs on OCT1, OCT2 and OCT3 activities were investigated using ASP^+, a reference substrate dye for OCTs (Fardel et al., 2015; Zhu et al., 2010). As expected, HEK-OCT1, HEK-OCT2 and HEK-OCT3 cells displayed marked increased accumulation of ASP^+ when compared to control HEK-MOCK and HEK-CTR cells (Figure 2A). Such uptakes of ASP^+ in HEK-OCT cells were moreover fully inhibited by reference OCT inhibitors (Figure 2A) and were saturable, with K_m values of 34.7 µM, 41.4 µM and 24.8 µM for HEK-OCT1, HEK-OCT2 and HEK-OCT3 cells, respectively (Figure 2B). Taken together, such data demonstrated that our transport assays based on ASP^+ uptake in HEK-OCT cells were fully relevant for analyzing OCT1, OCT2 and OCT3 activities.

The effects of two concentrations of HAAs, *i.e.*, 10 µM and 100 µM, were investigated towards OCT1, OCT2 and OCT3 activities (Figure 3); these two HAA concentrations were chosen because they are in the range of those previously used *in vitro* in various studies (Hashimoto et al., 2002; Naoi et al., 1989; Sayyed et al., 2017). When used at 10 µM, Trp-P-1, Trp-P-2 and harmane significantly reduced OCT1, OCT2 and OCT3 activity, whereas norharmane decreased only those of OCT1 and OCT2 and 7,8-diMeIQx those of OCT2 and OCT3. OCT2 activity was additionnally reduced by various HAAs used at 10 µM such as MeAαC, PhIP, Glu-P-2 and 4,8-diMeIQx and that of OCT3 by 10 µM Glu-P-1 (Figure 3). When used at 100 µM, the inhibitory effects of these HAAs towards OCT1, OCT2 and/or OCT3 activity were reinforced; residual activities of OCT1, OCT2 and OCT3 in HEK-OCT cells exposed to 100 µM Trp-P-1 or 100 µM Trp-P-2 notably represented less than 10 % of those found in untreated cells (Figure 3). OCT1 activity was also potently reduced by 100 µM MeIQ, as well as that of OCT2 by 100 µM harmane and 100 µM norharmane and that of OCT3 by 100 µM harmane and 100 µM 7,8-diMeIQx. For all HAAs inactive at 10 µM towards OCT2 or OCT3 activity, the use of 100 µM permitted to significantly inhibit them; by contrast, OCT1 activity remained not inhibited by AαC, PhIP, IQ and MeIQx when these HAAs were used at 100 µM (Figure 3).

Using the threshold of 50% transporter activity reduction, commonly admitted for defining drug transporter inhibition (Ahlin et al., 2008; De Bruyn et al., 2013; Kido et al., 2011), HAAs reaching it when used at 10 µM can be considered as potent inhibitors of OCTs (Table 2); it is notably the case for Trp-P-1 and Trp-P-2 towards OCT1, OCT2 and OCT3 and for harmane and norharmane towards OCT2. HAAs reaching the threshold of 50 % reduction when used only at 100 µM, such as Glu-P-1 and Glu-P-2 towards OCT2 and OCT3 activities, were classified as moderate OCT inhibitors (Table 2). HAAs which failed to significantly reduce OCT activity or

decreased it by less than 50% when used at 100 µM were finally considered as weak inhibitors or non-inhibitors (Table 2). Overall, OCT2 activity was the most impacted transporter by HAAs since all HAAs behave as potent or moderate inhibitors of this transporter (Table 2).

In order to investigate physico-chemical structural requirements for OCT inhibition by HAAs, inhibitions of OCT activities by HAAs were next confronted to values of various HAA molecular descriptors, through Pearson correlation analysis (Table 3). Some of these descriptors were significantly positively or negatively correlated to inhibition of only one OCT, like topological polar surface area (TPSA(Tot)), correlated to OCT2 inhibition (negative correlation), but not to those of OCT1 and OCT3 (Table 3). Other descriptors were correlated to inhibition of two OCTs, such as Ghose-Crippen octanol-water partition coefficient (logP) (ALOGP), positively correlated to OCT1 and OCT2 inhibitions, and the percentage of cationic form of HAAs at pH = 7.4, positively correlated with OCT1 and OCT3 inhibition. Only three molecular descriptors, *i.e.*, average molecular weight (AMW), maximum negative charge (qnmax) and submolecular polarity parameter (SPP), were correlated with OCT1, OCT2 and OCT3 inhibitions (Table 3).

3.2 Characterization of Trp-P-1 and Trp-P-2 interactions with OCTs

We next focused on interactions of Trp-P-1 and Trp-P-2 with OCT activities owing to the potent inhibitory effects of these two HAAs towards OCT1, OCT2 and OCT3 (Table 2). As indicated in Figure 4, the inhibition of OCT transporters by Trp-P-1 and Trp-P-2 was concentration-dependent, with IC_{50} values ranging from 1.9 µM (for OCT2 inhibition by Trp-P-2) to 6.5 µM (for OCT2 inhibition by Trp-P-1). Trp-P-1 and Trp-P-2 were next shown to inhibit OCT1-mediated uptake of TEA in human highly-differentiated hepatoma HepaRG cells, which constitutively express functional OCT1 (Le Vee et al., 2013); OCT1-mediated uptake of TEA was thus nearly fully abrogated by 100 µM Trp-P-1 and 100 µM Trp-P-2 (Figure 5), thus demonstrating that the

inhibitory effects of these two HAAs towards OCT1 were not restricted to OCT1-overexpressing HEK293 cells.

Because OCT1 and OCT2, unlike OCT3, are well-identified as playing a major role in xenobiotic disposition (Giacomini et al., 2010; Nies et al., 2011b), the putative transport of Trp-P-1 and Trp-P-2 by OCT1 and OCT2 was next investigated. For this purpose, we first analyzed whether the two HAAs may *trans*-stimulate [^{14}C]-TEA uptake in HEK-OCT1 and HEK-OCT2 cells, which may constitute an argument in favor of their transport by OCT1 and/or OCT2 (Grundemann et al., 2003; Zhang et al., 1999). Pre-loading with Trp-P-1 and Trp-P-2 however did not result in *trans*-stimulation of [^{14}C]-TEA uptake in both HEK-OCT1 and HEK-OCT2 cells, but rather in a *trans*-inhibition (Figure 6A). By contrast, pre-loading with unlabeled TEA *trans*-stimulated [^{14}C]-TEA uptake (Figure 6A), as expected for this OCT1/2 reference substrate (Zhang et al., 1999). We next compared the toxicity of Trp-P-1 and Trp-P-2 in HEK-MOCK, HEK-OCT1 and HEK-OCT2 cells, with the hypothesis that putative handling of the two HAAs by OCT1/OCT2 may enhance their toxicity through increasing their cellular uptake. As indicated in Figure 6B, the HAAs reduced cell viability of HEK-MOCK, HEK-OCT1 and HEK-OCT2 cells, in a concentration-dependent manner; IC_{50} values for Trp-P-1- and Trp-P-2-mediated alteration of cell viability however did not statistically differ between HEK-MOCK cells and HEK-OCT1 or HEK-OCT2 cells (Figure 6B). Accumulation of Trp-P-1 and Trp-P-2 was finally measured in HEK-MOCK, HEK-OCT1 and HEK-OCT2 cells using LC-MS/MS (Figure 6C). HEK-MOCK, HEK-OCT1 and HEK-OCT2 cells were found to exhibit similar cellular uptake of the two HAAs (Figure 6C); by contrast, HEK-OCT1 and HEK-OCT2 cells displayed much higher accumulations of the reference OCT substrate ASP^+ than HEK-MOCK cells (Figure 2A), thus confirming that OCT1 and OCT2 were fully functional.

3.3 Inhibition of non-OCT transporter activities by Trp-P-1 and Trp-P-2

To determine whether Trp-P-1 and Trp-P-2 may interact with other transporters than OCT1 and OCT2, we next analyzed their effect towards activities of three additional SLC transporters, *i.e.*, MATE1 and MATE2-K, expressed at the apical pole of hepatocytes and proximal tubular cells, respectively, and sharing numerous cationic substrates with OCTs (Nies et al., 2016; Nies et al., 2011b), and OATP1B1, involved in organic anion uptake at the sinusoidal pole of hepatocytes (Nies et al., 2013; Obaidat et al., 2012). Putative inhibition of two ABC transporters, *i.e.*, P-gp and BCRP, by the two HAAs was also studied. Such studies were performed using HEK-MATE1, HEK-MATE2-K, HEK-OATP1B1 and HEK-BCRP cells and P-gp-overexpressing MCF7R cells, which have been previously characterized with respect to reference substrate transport (Chedik et al., 2017; Jouan et al., 2016). As indicated in Figure 7, Trp-P-1 and Trp-P-2 significantly inhibited MATE1 and MATE2-K activity when used at 10 µM and 100 µM, the inhibition being more marked when the higher dose (100 µM) of HAA was used. With respect to OATP1B1 and BCRP activities, they were significantly reduced by 100 µM Trp-P-1 and 100 µM Trp-P-2, whereas the lower concentrations of 10 µM were ineffective. Whatever the concentrations (10 or 100 µM), the two HAAs failed to alter P-gp activity (Figure 7).

When applying the threshold of 50 % reduction of transporter activity described above for judging of a transporter inhibition, Trp-P-1 can be considered as a potent inhibitor of MATE1 and MATE2-K (inhibition by more than 50% of transporter activity at 10 µM), a moderate inhibitor of OATP1B1 and BCRP (inhibition by more than 50% of transporter activity at only 100 µM) and a non-inhibitor for P-gp (no inhibition or inhibition by less than 50% at 100 µM). Trp-P-2 appears as a potent inhibitor of MATE1, a moderate inhibitor of MATE2-K and a non-inhibitor of OATP1B1, BCRP and P-gp.

4. **Discussion**

The present study demonstrates that various HAAs can inhibit activity of OCT1, OCT2 and OCT3, thus adding OCTs to the list of drug transporters with which these carcinogenic contaminants interact. These inhibitions of OCT activities occur for the HAAs Trp-P-1 and Trp-P-2 at concentrations in the 2-6 µM range, which are much lower than concentrations in the 30-60 µM range required to exert cytotoxicity. This likely rules out the hypothesis that OCT inhibitions were the consequences of an unspecific major cellular toxicity of the HAAs. Moreover, the fact that Trp-P-1 and Trp-P-2 failed to inhibit P-gp-mediated transport, whereas they act as potent inhibitors of OCTs, likely discards the hypothesis of a non-specific and general inhibition of membrane transport processes by HAAs.

The exact profile of OCT activity inhibitions varies according to HAAs (Table 2). Thus, whereas 5/14 HAAs, *i.e.*, Trp-P-1, Trp-P-2, norharmane, MeIQ and 4,8-DiMeIQx, behave as inhibitors of OCT1, OCT2 and OCT3, other HAAs inhibit only one OCT, *i.e.*, OCT2 for AαC and MeAαC, or two OCTs, *i.e.*, OCT2 and OCT3 for PhIP, Glu-P-1, Glu-P-2, IQ, IQx, MeIQx and 7,8-DiMeIQx, or OCT1 and OCT2 for harmane (Table 2). The basis for such differential effects of HAAs towards activities of OCTs remains to be established, but it may be postulated to reflect variations in physico-chemical structures of HAAs. Indeed, physico-chemical properties of chemicals are known to constitute key-parameters governing their interactions with drug-binding sites of membrane transporters (Varma et al., 2017). In this context, correlations between various HAA molecular descriptors and OCT inhibitions were identified (Table 3). Some of them were common for the three OCTs: the molecular weight pondered by the number of atoms (average molecular weight/AMW) and the maximum negative charge (qnmax) were thus significantly negatively correlated to OCT1, OCT2 and OCT3 inhibition, whereas submolecular polarity

parameter (SPP), corresponding to the maximum excess charge difference for a pair of atoms in the molecule, was positively correlated. These data suggest that these descriptors may represent crucial parameters for common inhibition of OCT transporters by HAAs. This conclusion is supported for the two parameters related to the charge (qnmax and SPP) by the fact that charge has been previously recognized as one of the main parameters associated with OCT1 and OCT2 inhibition (Ahlin et al., 2008; Kido et al., 2011). In agreement with this assertion, various other molecular descriptors related to charge such as, for example, local dipole index (LDI), partial charge weighted topological electronic index (PCWTE1), relative negative charge (RNCG), maximum positive charge (qpmax), mean absolute charge (charge polarization) (Qmean) and the percentage of cationic form at pH = 7.4 were also significantly correlated with OCT1, OCT2 and/or OCT3 inhibitions by HAAs (Table 3). The relationship with the charge is additionally reinforced by the fact that the potent OCT inhibitors Trp-P-1 and Trp-P-2 are the most basic amines among the fifteen HAAs included in the present study; they therefore display the highest predicted percentages of cationic form at pH = 7.4 (99.73% and 99.49%, respectively) (data not shown). Besides charge-related parameters, Ghose-Crippen octanol-water partition coefficient/logP (ALOGP) was correlated with OCT1 and OCT2 inhibition by HAAs, which agrees with the previous conclusion that lipophilicity is associated with OCT1 and OCT2 inhibition (Ahlin et al., 2008; Kido et al., 2011). By contrast, ALOGP was not significantly correlated with OCT3 inhibition by HAAs, which does not support a role for lipophilicity for OCT3 inhibition. Analysis of a large data set of structurally-diverse chemicals with respect to OCT3 inhibition is however required to confirm this hypothesis. Similar studies have also to be considered for determining whether the implication in OCT inhibition of other descriptors such as, for example, the number

of pyrroles (nPyrroles) or the number of imidazoles (nImidazoles) (Table 3), may be generalizable to other chemicals than HAAs.

The *in vivo* relevance of OCT inhibition by HAAs and its putative consequences remain to be established. It may be postulated that the inhibition of OCTs by HAAs may block the transport of endogenous OCT substrates, especially that of catecholamines, known to act as neurotransmitters. By this way, OCT inhibition may contribute to the possible neurotoxicity of HAAs, including PhIP, Trp-P-1 and Trp-P-2 (Cruz-Hernandez et al., 2018; Naoi et al., 1989). In particular, OCT inhibition by harmane and norharmane may be involved in the neurological diseases thought to be promoted by these two HAAs, such as essential tremor and the Parkinson disease (Esmaeili et al., 2012; Lavita et al., 2016). Whether HAAs may *in vivo* reach concentrations required for inhibiting activities of OCTs remains however a key-point to consider. In this context, blood harmane concentrations in humans have been reported to be in the 0.2-0.3 ng/mL range (Louis et al., 2013), *i.e.*, in the 1.1-1.6 nM range, whereas IC_{50} value of harmane towards OCT2 activity in HEK-OCT2 cells is 1.3 ± 0.1 µM (data not shown), thus indicating that harmane blood concentrations are very unlikely to block OCT2 activity *in vivo*. In the same way, the amounts of Trp-P-2 found in one cigarette is in the 2.8-5.3 ng range (Zhang et al., 2011), which corresponds to a theoretical blood concentration of approximately 2.8-5.4 pM if retaining the hypothesis that Trp-P-2 is totally absorbed at the lung level and subsequently freely diffuses into the whole blood compartment, whose volume is set at 5 L. Putative *in vivo* Trp-P-2 concentrations in smokers are therefore likely in the pM range, far less than the 2-6 µM range of concentrations required to inhibit OCT1, OCT2 or OCT3 activity. This suggests that blood concentrations of HAAs occurring in response to smoking are unlikely to cause OCT inhibition. With respect to dietary HAAs, their daily uptake is estimated to be rather low in general, *i.e.*, it does not exceed the amount of 1 µg per

person on average (Keating and Bogen, 2004). In particular, the absorbed intestinal amount of PhIP and MeIQx, which are the most abundant HAAs produced during cooking of meat (Zhang et al., 2013), can be estimated to reach approximately 1 µg after a meal with fried meat (Reistad et al., 1997), which can theoretically result in 0.5-1 nM blood concentrations, knowing that hepatic metabolism of HAAs probably reduces such levels in a notable way. These hypothetical blood concentrations of PhIP and MeIQx are much less than the 100 µM concentration required to inhibit OCT2 and OCT3 activities (Figure 3), thus suggesting that dietary HAAs may fail to inhibit OCTs-mediated transport *in vivo*. This assertion has however to be challenged by the fact that humans are usually simultaneously exposed to various HAAs, whose inhibitory effects towards OCTs may synergize, as already demonstrated for other chemical contaminants (Chedik et al., 2018). In addition, local concentrations of HAAs in the gastrointestinal tract may be hypothesized to be much higher than HAA concentrations in the blood; this may support the idea that OCTs present in intestine and liver, such as OCT1 and OCT3, expressed at the sinusoidal pole of hepatocytes (Nies et al., 2009) and apical pole of enterocytes (Han et al., 2013), may be locally targeted by dietary HAAs.

It is noteworthy that the HAAs Trp-P-1 and Trp-P-2 are not transported by OCT1 and OCT2, because (i) they failed to *trans*-stimulate OCT1 and OCT2 activities, (ii) they exerted the same cytotoxicity in HEK-MOCK, HEK-OCT1 and HEK-OCT2 cells and (iii) they similarly accumulated in HEK-MOCK, HEK-OCT1 and HEK-OCT2 cells. These HAAs thus behave as inhibitors of OCT1 and OCT2, without being transported, thus excluding any major contribution of OCT1 and OCT2 to their systemic toxicokinetics. Other pollutants interacting with OCT1 and OCT2 such as pyrethroids and organophosphorus pesticides are similarly not transported by these SLC uptake transporters (Chedik et al., 2018; Chedik et al., 2017).

In addition to inhibiting OCT1, OCT2 and OCT3 activities, Trp-P-1 and Trp-P-2 decreased those of the SLC transporters MATE1 and MATE2-K, when used either at 10 or 100 µM. Such a notable inhibition of MATEs is not surprising because MATEs share numerous inhibitors and substrates, including organic cations, with OCTs (Nies et al., 2016; Nies et al., 2011b). Trp-P-1 and Trp-P-2 also blocked BCRP activity, but only when used at 100 µM; this interaction with this ABC efflux pump agrees with the fact that at least Trp-P-1 has been previously shown to be transported by BCRP (van Herwaarden et al., 2006). OATP1B1 activity was additionally reduced by 100 µM Trp-P-1 and 100 µM Trp-P-2, suggesting that organic anion transporters are also targeted by HAAs. The fact that Trp-P-2, as well as PhIP and AαC, inhibited OAT3 activity (Sayyed et al., 2017), fully supports this conclusion. Whether OATP1B1 may transport some HAAs would deserve additional studies. Finally, the interactions of HAAs with OCTs and other transporters, associated with the estrogenic activity of PhIP (Lauber and Gooderham, 2007), as well as the inhibitory effects towards enzymes and the activation of xenobiotic-sensing receptor like the aryl hydrocarbon receptor by some HAAs (Dumont et al., 2010; Naoi et al., 1988), highlight the fact that these chemicals, mainly known as genotoxic compounds, can exert diverse cellular and molecular effects not related to genotoxicity. Further studies may be useful to evaluate the exact contribution of these non-genotoxic effects to HAAs overall toxicity.

In summary, HAAs were shown to inhibit activities of OCTs *in vitro*, without, at least for Trp-P-1 and Trp-P-2, being transported by OCT1 and OCT2. Such data support the conclusion that interactions with membrane transporters are not restricted to drugs, but also concern environmental chemical contaminants like HAAs, bisphenols (Bruyere et al., 2017) or pesticides (Bain and LeBlanc, 1996; Chedik et al., 2017). The *in vivo* relevance of pollutants-mediated inhibition of transporter activities remains however challenged by the fact that human exposure to

most of pollutants may result in tissue and blood levels of pollutants probably too low to be active on *in vivo* drug transporter activities.

Acknowledgements

The authors thank Dr Y. Parmentier and Dr C. Denizot, for helpful support with HEK293 cell clones overexpressing transporters, and Technologie Servier (Orléans, France), for the gift of the LC-MS/MS system. K. Sayyed was the recipient of a grant from AZM Association-UL (Tripoli, Lebanon). Dr A.T. Nies was supported by the Robert-Bosch Foundation (Stuttgart, Germany) and the Interfaculty Centre for Pharmacogenomics and Pharma Research (ICEPHA) Grant (Tübingen-Stuttgart, Germany).

References

Ahlin, G., Karlsson, J., Pedersen, J.M., Gustavsson, L., Larsson, R., Matsson, P., Norinder, U., Bergstrom, C.A., Artursson, P., 2008. Structural requirements for drug inhibition of the liver specific human organic cation transport protein 1. J Med Chem 51, 5932-5942.

Bain, L.J., LeBlanc, G.A., 1996. Interaction of structurally diverse pesticides with the human MDR1 gene product P-glycoprotein. Toxicol Appl Pharmacol 141, 288-298.

Bradford, M.M., 1976. A rapid and sensitive method for the quantitation of microgram quantities of protein utilizing the principle of protein-dye binding. Anal Biochem 72, 248-254.

Bruyere, A., Hubert, C., Le Vee, M., Chedik, L., Sayyed, K., Stieger, B., Denizot, C., Parmentier, Y., Fardel, O., 2017. Inhibition of SLC drug transporter activities by environmental bisphenols. Toxicol In Vitro 40, 34-44.

Carmichael, J., DeGraff, W.G., Gazdar, A.F., Minna, J.D., Mitchell, J.B., 1987. Evaluation of a tetrazolium-based semiautomated colorimetric assay: assessment of chemosensitivity testing. Cancer Res 47, 936-942.

Chedik, L., Bruyere, A., Fardel, O., 2018. Interactions of organophosphorus pesticides with solute carrier (SLC) drug transporters. Xenobiotica, 1-12.

Chedik, L., Bruyere, A., Le Vee, M., Stieger, B., Denizot, C., Parmentier, Y., Potin, S., Fardel, O., 2017. Inhibition of Human Drug Transporter Activities by the Pyrethroid Pesticides Allethrin and Tetramethrin. PLoS One 12, e0169480.

Cheng, K.W., Chen, F., Wang, M., 2006. Heterocyclic amines: chemistry and health. Mol Nutr Food Res 50, 1150-1170.

Coles, B., Nowell, S.A., MacLeod, S.L., Sweeney, C., Lang, N.P., Kadlubar, F.F., 2001. The role of human glutathione S-transferases (hGSTs) in the detoxification of the food-derived carcinogen metabolite N-acetoxy-PhIP, and the effect of a polymorphism in hGSTA1 on colorectal cancer risk. Mutat Res 482, 3-10.

Cruz-Hernandez, A., Agim, Z.S., Montenegro, P.C., McCabe, G.P., Rochet, J.C., Cannon, J.R., 2018. Selective dopaminergic neurotoxicity of three heterocyclic amine subclasses in primary rat midbrain neurons. Neurotoxicology 65, 68-84.

De Bruyn, T., van Westen, G.J., Ijzerman, A.P., Stieger, B., de Witte, P., Augustijns, P.F., Annaert, P.P., 2013. Structure-based identification of OATP1B1/3 inhibitors. Mol Pharmacol 83, 1257-1267.

Dietrich, C.G., de Waart, D.R., Ottenhoff, R., Schoots, I.G., Elferink, R.P., 2001. Increased bioavailability of the food-derived carcinogen 2-amino-1-methyl-6-phenylimidazo[4,5-b]pyridine in MRP2-deficient rats. Mol Pharmacol 59, 974-980.

Dumont, J., Josse, R., Lambert, C., Antherieu, S., Laurent, V., Loyer, P., Robin, M.A., Guillouzo, A., 2010. Preferential induction of the AhR gene battery in HepaRG cells after a single or repeated exposure to heterocyclic aromatic amines. Toxicol Appl Pharmacol 249, 91-100.

Esmaeili, M.H., Movahedi, M., Faraji, A., Haghdoost-Yazdi, H., 2012. Intracerebral injection of low amounts of norharman induces moderate Parkinsonism-like behavioral symptoms in rat. Neurotoxicol Teratol 34, 489-494.

Fardel, O., Le Vee, M., Jouan, E., Denizot, C., Parmentier, Y., 2015. Nature and uses of fluorescent dyes for drug transporter studies. Expert Opin Drug Metab Toxicol 11, 1233-1251.

Giacomini, K.M., Huang, S.M., Tweedie, D.J., Benet, L.Z., Brouwer, K.L., Chu, X., Dahlin, A., Evers, R., Fischer, V., Hillgren, K.M., Hoffmaster, K.A., Ishikawa, T., Keppler, D., Kim, R.B., Lee, C.A., Niemi, M., Polli, J.W., Sugiyama, Y., Swaan, P.W., Ware, J.A., Wright, S.H., Yee, S.W., Zamek-Gliszczynski, M.J., Zhang, L., 2010. Membrane transporters in drug development. Nat Rev Drug Discov 9, 215-236.

Gripon, P., Rumin, S., Urban, S., Le Seyec, J., Glaise, D., Cannie, I., Guyomard, C., Lucas, J., Trepo, C., Guguen-Guillouzo, C., 2002. Infection of a human hepatoma cell line by hepatitis B virus. Proc Natl Acad Sci U S A 99, 15655-15660.

Grundemann, D., Hahne, C., Berkels, R., Schomig, E., 2003. Agmatine is efficiently transported by non-neuronal monoamine transporters extraneuronal monoamine transporter (EMT) and organic cation transporter 2 (OCT2). J Pharmacol Exp Ther 304, 810-817.

Grundemann, D., Liebich, G., Kiefer, N., Koster, S., Schomig, E., 1999. Selective substrates for non-neuronal monoamine transporters. Mol Pharmacol 56, 1-10.

Han, T.K., Everett, R.S., Proctor, W.R., Ng, C.M., Costales, C.L., Brouwer, K.L., Thakker, D.R., 2013. Organic cation transporter 1 (OCT1/mOct1) is localized in the apical membrane of Caco-2 cell monolayers and enterocytes. Mol Pharmacol 84, 182-189.

Hashimoto, T., Furuyashiki, T., Sano, T., Ito, W., Danno, G., Kanazawa, K., Ashida, H., 2002. 3-amino-1,4-dimethyl-5H-pyrido[4,3-b]indole (trp-P-1) is incorporated into rat splenocytes, thymocytes, and hepatocytes through monoamine transporters and induces apoptosis. Biosci Biotechnol Biochem 66, 1205-1212.

Jonker, J.W., Schinkel, A.H., 2004. Pharmacological and physiological functions of the polyspecific organic cation transporters: OCT1, 2, and 3 (SLC22A1-3). J Pharmacol Exp Ther 308, 2-9.

Jouan, E., Le Vee, M., Denizot, C., Da Violante, G., Fardel, O., 2014. The mitochondrial fluorescent dye rhodamine 123 is a high-affinity substrate for organic cation transporters (OCTs) 1 and 2. Fundam Clin Pharmacol 28, 65-77.

Jouan, E., Le Vee, M., Mayati, A., Denizot, C., Parmentier, Y., Fardel, O., 2016. Evaluation of P-Glycoprotein Inhibitory Potential Using a Rhodamine 123 Accumulation Assay. Pharmaceutics 8.

Keating, G.A., Bogen, K.T., 2004. Estimates of heterocyclic amine intake in the US population. J Chromatogr B Analyt Technol Biomed Life Sci 802, 127-133.

Kido, Y., Matsson, P., Giacomini, K.M., 2011. Profiling of a prescription drug library for potential renal drug-drug interactions mediated by the organic cation transporter 2. J Med Chem 54, 4548-4558.

Langouet, S., Welti, D.H., Kerriguy, N., Fay, L.B., Huynh-Ba, T., Markovic, J., Guengerich, F.P., Guillouzo, A., Turesky, R.J., 2001. Metabolism of 2-amino-3,8-dimethylimidazo[4,5-

f]quinoxaline in human hepatocytes: 2-amino-3-methylimidazo[4,5-f]quinoxaline-8-carboxylic acid is a major detoxification pathway catalyzed by cytochrome P450 1A2. Chem Res Toxicol 14, 211-221.

Lauber, S.N., Gooderham, N.J., 2007. The cooked meat derived genotoxic carcinogen 2-amino-3-methylimidazo[4,5-b]pyridine has potent hormone-like activity: mechanistic support for a role in breast cancer. Cancer Res 67, 9597-9602.

Lavita, S.I., Aro, R., Kiss, B., Manto, M., Duez, P., 2016. The Role of beta-Carboline Alkaloids in the Pathogenesis of Essential Tremor. Cerebellum 15, 276-284.

Le Vee, M., Jouan, E., Stieger, B., Lecureur, V., Fardel, O., 2015. Regulation of human hepatic drug transporter activity and expression by diesel exhaust particle extract. PLoS One 10, e0121232.

Le Vee, M., Noel, G., Jouan, E., Stieger, B., Fardel, O., 2013. Polarized expression of drug transporters in differentiated human hepatoma HepaRG cells. Toxicol In Vitro 27, 1979-1986.

Louis, E.D., Benito-Leon, J., Moreno-Garcia, S., Vega, S., Romero, J.P., Bermejo-Pareja, F., Gerbin, M., Viner, A.S., Factor-Litvak, P., Jiang, W., Zheng, W., 2013. Blood harmane (1-methyl-9H-pyrido[3,4-b]indole) concentration in essential tremor cases in Spain. Neurotoxicology 34, 264-268.

Mosmann, T., 1983. Rapid colorimetric assay for cellular growth and survival: application to proliferation and cytotoxicity assays. Journal of immunological methods 65, 55-63.

Naoi, M., Takahashi, T., Ichinose, H., Wakabayashi, K., Sugimura, T., Nagatsu, T., 1988. Reduction of enzyme activity of tyrosine hydroxylase and aromatic L-aminoacid

decarboxylase in clonal pheochromocytoma PC12h cells by carcinogenic heterocyclic amines. Biochem Biophys Res Commun 157, 494-499.

Naoi, M., Takahashi, T., Ichinose, H., Wakabayashi, K., Sugimura, T., Nagatsu, T., 1989. Uptake of heterocyclic amines, Trp-P-1 and Trp-P-2, into clonal rat pheochromocytoma PC12h cells by dopamine uptake system. Neurosci Lett 99, 317-322.

Nies, A.T., Damme, K., Kruck, S., Schaeffeler, E., Schwab, M., 2016. Structure and function of multidrug and toxin extrusion proteins (MATEs) and their relevance to drug therapy and personalized medicine. Arch Toxicol 90, 1555-1584.

Nies, A.T., Hofmann, U., Resch, C., Schaeffeler, E., Rius, M., Schwab, M., 2011a. Proton pump inhibitors inhibit metformin uptake by organic cation transporters (OCTs). PLoS One 6, e22163.

Nies, A.T., Koepsell, H., Damme, K., Schwab, M., 2011b. Organic cation transporters (OCTs, MATEs), in vitro and in vivo evidence for the importance in drug therapy. Handb Exp Pharmacol, 105-167.

Nies, A.T., Koepsell, H., Winter, S., Burk, O., Klein, K., Kerb, R., Zanger, U.M., Keppler, D., Schwab, M., Schaeffeler, E., 2009. Expression of organic cation transporters OCT1 (SLC22A1) and OCT3 (SLC22A3) is affected by genetic factors and cholestasis in human liver. Hepatology 50, 1227-1240.

Nies, A.T., Niemi, M., Burk, O., Winter, S., Zanger, U.M., Stieger, B., Schwab, M., Schaeffeler, E., 2013. Genetics is a major determinant of expression of the human hepatic uptake transporter OATP1B1, but not of OATP1B3 and OATP2B1. Genome Med 5, 1.

Obaidat, A., Roth, M., Hagenbuch, B., 2012. The expression and function of organic anion transporting polypeptides in normal tissues and in cancer. Annu Rev Pharmacol Toxicol 52, 135-151.

Reistad, R., Rossland, O.J., Latva-Kala, K.J., Rasmussen, T., Vikse, R., Becher, G., Alexander, J., 1997. Heterocyclic aromatic amines in human urine following a fried meat meal. Food Chem Toxicol 35, 945-955.

Sayyed, K., Le Vee, M., Abdel-Razzak, Z., Fardel, O., 2017. Inhibition of organic anion transporter (OAT) activity by cigarette smoke condensate. Toxicol In Vitro 44, 27-35.

Shimada, T., Hayes, C.L., Yamazaki, H., Amin, S., Hecht, S.S., Guengerich, F.P., Sutter, T.R., 1996. Activation of chemically diverse procarcinogens by human cytochrome P-450 1B1. Cancer Res 56, 2979-2984.

Stillwell, W.G., Turesky, R.J., Sinha, R., Tannenbaum, S.R., 1999. N-oxidative metabolism of 2-amino-3,8-dimethylimidazo[4,5-f]quinoxaline (MeIQx) in humans: excretion of the N2-glucuronide conjugate of 2-hydroxyamino-MeIQx in urine. Cancer Res 59, 5154-5159.

Sugimura, T., Wakabayashi, K., Nakagama, H., Nagao, M., 2004. Heterocyclic amines: Mutagens/carcinogens produced during cooking of meat and fish. Cancer Sci 95, 290-299.

Talhout, R., Schulz, T., Florek, E., van Benthem, J., Wester, P., Opperhuizen, A., 2011. Hazardous compounds in tobacco smoke. Int J Environ Res Public Health 8, 613-628.

Tournier, N., Chevillard, L., Megarbane, B., Pirnay, S., Scherrmann, J.M., Decleves, X., 2010. Interaction of drugs of abuse and maintenance treatments with human P-glycoprotein (ABCB1) and breast cancer resistance protein (ABCG2). Int J Neuropsychopharmacol 13, 905-915.

Turesky, R.J., 2002. Heterocyclic aromatic amine metabolism, DNA adduct formation, mutagenesis, and carcinogenesis. Drug Metab Rev 34, 625-650.

Turesky, R.J., 2007. Formation and biochemistry of carcinogenic heterocyclic aromatic amines in cooked meats. Toxicol Lett 168, 219-227.

Turesky, R.J., Le Marchand, L., 2011. Metabolism and biomarkers of heterocyclic aromatic amines in molecular epidemiology studies: lessons learned from aromatic amines. Chem Res Toxicol 24, 1169-1214.

van Herwaarden, A.E., Jonker, J.W., Wagenaar, E., Brinkhuis, R.F., Schellens, J.H., Beijnen, J.H., Schinkel, A.H., 2003. The breast cancer resistance protein (Bcrp1/Abcg2) restricts exposure to the dietary carcinogen 2-amino-1-methyl-6-phenylimidazo[4,5-b]pyridine. Cancer Res 63, 6447-6452.

van Herwaarden, A.E., Wagenaar, E., Karnekamp, B., Merino, G., Jonker, J.W., Schinkel, A.H., 2006. Breast cancer resistance protein (Bcrp1/Abcg2) reduces systemic exposure of the dietary carcinogens aflatoxin B1, IQ and Trp-P-1 but also mediates their secretion into breast milk. Carcinogenesis 27, 123-130.

Varma, M.V., Lai, Y., El-Kattan, A.F., 2017. Molecular properties associated with transporter-mediated drug disposition. Adv Drug Deliv Rev 116, 92-99.

Vlaming, M.L., Teunissen, S.F., van de Steeg, E., van Esch, A., Wagenaar, E., Brunsveld, L., de Greef, T.F., Rosing, H., Schellens, J.H., Beijnen, J.H., Schinkel, A.H., 2014. Bcrp1;Mdr1a/b;Mrp2 combination knockout mice: altered disposition of the dietary carcinogen PhIP (2-amino-1-methyl-6-phenylimidazo[4,5-b]pyridine) and its genotoxic metabolites. Mol Pharmacol 85, 520-530.

Walle, U.K., Walle, T., 1999. Transport of the cooked-food mutagen 2-amino-1-methyl-6-phenylimidazo-[4,5-b]pyridine (PhIP) across the human intestinal Caco-2 cell monolayer: role of efflux pumps. Carcinogenesis 20, 2153-2157.

Zhang, L., Ashley, D.L., Watson, C.H., 2011. Quantitative analysis of six heterocyclic aromatic amines in mainstream cigarette smoke condensate using isotope dilution liquid chromatography-electrospray ionization tandem mass spectrometry. Nicotine Tob Res 13, 120-126.

Zhang, L., Gorset, W., Dresser, M.J., Giacomini, K.M., 1999. The interaction of n-tetraalkylammonium compounds with a human organic cation transporter, hOCT1. J Pharmacol Exp Ther 288, 1192-1198.

Zhang, Y., Yu, C., Mei, J., Wang, S., 2013. Formation and mitigation of heterocyclic aromatic amines in fried pork. Food Addit Contam Part A Chem Anal Control Expo Risk Assess 30, 1501-1507.

Zhou, F., Zhu, L., Wang, K., Murray, M., 2017. Recent advance in the pharmacogenomics of human Solute Carrier Transporters (SLCs) in drug disposition. Adv Drug Deliv Rev 116, 21-36.

Zhu, H.J., Appel, D.I., Grundemann, D., Markowitz, J.S., 2010. Interaction of organic cation transporter 3 (SLC22A3) and amphetamine. J Neurochem 114, 142-149.

Legends to figures

Figure 1. Chemical structures of HAAs included in the study.

Figure 2. Characterization of ASP^+ uptake in HEK-OCT1, HEK-OCT2 and HEK-OCT3 cells.

(A) HEK-OCT1, HEK-OCT2, HEK-OCT3, HEK-MOCK and HEK-CTR cells were incubated with 10 µM ASP^+ for 5 min at 37°C in the absence (untreated) or presence of reference OCT inhibitors (amitriptyline used at 200 µM for OCT1 or at 100 µM for OCT2, and 100 µM corticosterone for OCT3). (B) HEK-OCT1, HEK-OCT2 and HEK-OCT3 cells were incubated with various concentrations of ASP^+ (from 1 to 100 µM) for 5 min at 37°C. (A, B) Intracellular accumulation of ASP^+ was next determined by spectrofluorimetry and normalized to protein content. Data are the means ± SEM of three independent assays. (A) *, $p<0.05$; ns, not statistically significant. (B) Kinetic parameters (K_m and V_{max}) are indicated at the top of graphs. FAU, fluorescence arbitrary unit.

Figure 3. Effects of various HAAs on OCT1, OCT2 and OCT3 activities.

HEK-OCT1, HEK-OCT2 and HEK-OCT3 cells were incubated with 10 µM ASP^+ for 5 min at 37°C in the absence (untreated) or presence of various HAAs used at 10 µM and 100 µM. Intracellular accumulation of ASP^+ was next determined by spectrofluorimetry and normalized to protein content. Data are expressed as % of OCT activity found in untreated cells, arbitrarily set at 100 % and indicated by a dashed line on the graphs; they are the means ± SEM of at least three independent experiments. *, $p<0.05$ when compared to untreated cells.

Figure 4. Concentration-dependent inhibition of OCT1, OCT2 and OCT3 activities by Trp-P-1 and Trp-P-2.

HEK-OCT1, HEK-OCT2 and HEK-OCT3 cells were incubated with 10 µM ASP^+ for 5 min at 37°C in the absence or presence of various concentrations (from 0.01 µM to 300 µM) of Trp-P-1 and Trp-P-2. Intracellular accumulation of ASP^+ was next determined by spectrofluorimetry and normalized to protein content. Data are expressed as % of OCT activity found in untreated cells, arbitrarily set at 100 %; they are the means ± SEM of at least three independent experiments. Trp-P-1 and Trp-P-2 IC_{50} values are indicated on the top of graphs.

Figure 5. Effect of Trp-P-1 and Trp-P-2 on OCT1 activity in human hepatoma HepaRG cells. HepaRG cells were incubated for 10 min at 37°C with the OCT1 reference substrate [^{14}C]-TEA, in the absence (untreated) or presence of Trp-P-1 or Trp-P-2 (used both at 10 and 100 µM) or of the reference inhibitor verapamil (50 µM). Intracellular accumulation of [^{14}C]-TEA was then determined by scintillation counting. Data are expressed as % of OCT1-mediated [^{14}C]-TEA uptake found in untreated cells, arbitrarily set at 100% and indicated by a dashed line on the graph; they are the means ± SEM of three independent assays. *, $p < 0.05$ when compared to untreated cells.

Figure 6. *Trans*-stimulation effects (A), toxicity (B) and accumulation (C) of Trp-P-1 and Trp-P-2 in HEK-OCT1 and HEK-OCT2 cells.

(A) HEK-OCT1 and HEK-OCT2 cells were first incubated with 2 mM unlabeled TEA or 100 µM of Trp-P-1 or Trp-P-2 cells for 60 min at 37°C. After washing with PBS, cells were next re-incubated with radiolabeled [^{14}C]-TEA (used at 28.6 µM) for 5 min at 37°C. Intracellular accumulation of radiolabeled TEA was finally determined by scintillation counting. Data were expressed as percentages of [^{14}C]-TEA accumulation found in control untreated cells, arbitrarily

set at 100% and indicated by a dashed line on the graph; they are the means ± SEM of three independent assays. *, p <0.05 when compared to untreated cells. (B) Confluent HEK-MOCK, HEK-OCT1 and HEK-OCT2 cells were either untreated or treated by various concentrations (from 0.3 to 300 µM) of Trp-P-1 and Trp-P-2 for 24 h. Cellular viability was next determined using the MTT assay. Data are expressed as % of viability found in untreated cells, set at 100%; they are the means ± SEM of three independent assays. Trp-P-1 and Trp-P-2 IC_{50} values towards viability are indicated at top of the graphs; ns, not statistically significant when compared to IC_{50} value found in HEK-MOCK cells. (C) HEK-MOCK, HEK-OCT1 and HEK-OCT2 cells were incubated with 1 µM Trp-P-1 or 1 µM Trp-P-2, for 10 min at 37°C. Intracellular accumulation of the two HAAs were then determined by LC-MS/MS. Data are the means ± SEM of four independent assays. ns, not statistically significant when compared to HEK-MOCK cells.

Figure 7. Effects of Trp-P-1 and Trp-P-2 on MATE1, MATE2-K, OATP1B1, P-gp and BCRP activities.

Effects of Trp-P-1 and Trp-P-2, each used at 10 and 100 µM, on MATE1, MATE2-K, OATP1B1, BCRP and P-gp activities were determined in HEK-MATE1, HEK-MATE2-K, HEK-OATP1B1 and HEK-BCRP cells and in P-gp-overexpressing MCF7R cells, as described in Materials and Methods. Data are expressed as % of transport activity found in HAAs-untreated cells, arbitrarily set at 100 % and indicated by a dashed line on the graphs; they are the means ± SEM of at least three independent experiments. *, p<0.05 when compared to untreated cells.

Table 1. List of HAAs analyzed in the study

Short name	Complete chemical name	Class
AαC	2-amino-9H-pyrido[2,3-b]indole	Pyrolytic
4,8-diMeIQx	2-amino-3,7,8 trimethylimidazo[4,5-f]quinoxaline	Thermic
7,8-diMeIQx	2-amino-3,4,8-trimethylimidazo[4,5-f]quinoxaline	Thermic
Glu-P-1	2-amino-6-methyl[1,2-a:3',2''-d]imidazole	Pyrolytic
Glu-P-2	2-aminodipyrido[1,2-a:3',2''-d]imidazole	Pyrolytic
Harmane	methyl-9H-pyrido[3,4-b]indole	Pyrolytic
IQ	2-amino-3-methyl-imidazo [4, 5-f] quinoline	Thermic
IQx	2-amino-3-méthyl-3H-imidazo[4,5-f]quinoxaline	Thermic
MeAαC	2-amino-3-methyl-9H-pyrido[2,3-b]indole	Pyrolytic
MeIQ	2-amino-3,4-dimethyl-3H imidazo[4,5-f]quinoline	Thermic
MeIQx	2-amino-3,8-dimethylimidazo[4,5-f]quinoxaline	Thermic
Norharmane	9H-pyrido[3,4-b]indole	Pyrolytic
PhIP	2-amino-1-methyl-6-phenylimidazo(4,5-b)pyridine	Thermic
Trp-P-1	3-amino-1,4-dimethyl-5H-pyrido [4,3-b]indole	Pyrolytic
Trp-P-2	3-amino-1-methyl-5H-pyrido[4,3-b]-indole	Pyrolytic

Table 2. Summary of HAA effects towards OCT activities

HAA	Inhibition potency towards OCT activity[a]		
	OCT1	OCT2	OCT3
AαC	-	+	-
4,8-DiMeIQx	+	+	+
7,8-DiMeIQx	-	++	++
Glu-P-1	-	+	+
Glu-P-2	-	+	+
Harmane	++	++	-
IQ	-	+	+
IQx	-	+	+
MeAαC	-	+	-
MeIQ	+	+	+
MeIQx	-	+	+
Norharmane	+	++	+
PhIP	-	+	+
Trp-P-1	++	++	++
Trp-P-2	++	++	++

[a] The cut-off was 50% of reduction of transporter activity by HAAs. ++, potent inhibition (more than 50% when HAA is used at 10 µM); +, moderate inhibition (more than 50 % only when HAA is used at 100 µM); -, no inhibition or inhibition by less than 50% when HAA is used at 100 µM.

Table 3. List of HAA molecular descriptors correlated with OCT activity inhibition by 10 μM HAAs

Molecular descriptor		Activity inhibition		
Block	Name	OCT1	OCT2	OCT3
Constitutional indices (n = 47)[a]	average molecular weight (AMW)	r = -0.623, p = 0.012	r = -0.534, p = 0.040	r= -0.608, p = 0.016
	mean atomic Sanderson electronegativity (scaled on carbon atom) (Me)	r = -0.731, p = 0.002	r = -0.786, p = 0.0005	Not correlated
	mean first ionization potential (scaled on carbon atom) (Mi)	Not correlated	r = -0.6493, p = 0.009	Not correlated
	number of carbon atoms (nc)	Not correlated	r = 0.521, p = 0.046	r = 0.532, p=0.041
	number of nitrogen atoms (nN)	r = -0.585, p = 0.022	r = -0.670, p = 0.006	Not correlated
	number of heteroatoms (nHet)	r = -0.585, p = 0.022	r = -0.670, p = 0.006	Not correlated
	percentage of H atoms (H%)	r = 0.521, p = 0.046	Not correlated	r = 0.576, p = 0.024
	percentage of C atoms (C%)	Not correlated	r = 0.542, p = 0.037	Not correlated
	percentage of N atoms (N%)	r = -0.697, p = 0.004	r = -0.784, p = 0.0005	Not correlated
Functional group counts (n = 154)[a]	number of terminal primary C(sp3) (ncp)	Not correlated	Not correlated	r = 0.554, p = 0.032
	number of primary amines (aromatic) (nArNH2)	Not correlated	r = -0.596, p = 0.019	Not correlated
	number of pyrroles (nPyrroles)	r = 0.678, p= 0.005	r = 0.602, p = 0.017	Not correlated
	number of Imidazoles (nImidazoles)	r = -0.678, p = 0.005	r = -0.602, p = 0.017	Not correlated
	number of acceptor atoms for H-bonds (N,O,F) (nHAcc)	r = -0.586, p = 0.022	r = -0.670, p = 0.006	Not correlated
Charge descriptors (n = 16)[a]	maximum positive charge (qpmax)	r = 0.670, p = 0.006	r = 0.589, p = 0.0209	Not correlated
	maximum negative charge (qnmax)	r = -0.845, p<0.0001	r = -0.544, p = 0.036	r = -0.662, p = 0.007
	mean absolute charge (charge polarization) (Qmean)	Not correlated	r = -0.619, p = 0.014	Not correlated
	relative positive charge (RPCG)	Not correlated	r = 0.624, p = 0.013	Not correlated
	relative negative charge (RNCG)	r = 0.672, p = 0.006	r = 0.679, p = 0.0054	Not correlated
	submolecular polarity parameter (SPP)	r = 0.822, p = 0.0002	r = 0.5829, p = 0.023	r = 0.559, p = 0.030
	topographic electronic descriptor (bond resctricted) (TE2)	Not correlated	r = -0.655, p = 0.008	Not correlated
	partial charge weighted topological electronic index (PCWTE1)	r = -0.576, p = 0.025	r = -0.599, p = 0.018	Not correlated
	partial charge weighted topological electronic index (bond restricted) (PCWTE2)	r = -0.729, p = 0.002	r = -0.735, p = 0.002	Not correlated
	local dipole index (LDI)	r = -0.620, p = 0.014	r = - 0.824, p = 0.0002	Not correlated
	% of cationic form at pH = 7.4	r = 0.767, p = 0.0008	Not correlated	r=0.748, p=0.001
Molecular properties (n = 20)[a]	topological polar surface area using N,O polar contributions (TPSA(NO))	Not correlated	r = -0.657, p = 0.008	Not correlated
	topological polar surface area using N,O,S,P polar contributions (TPSA(Tot))	Not correlated	r = -0.657, p = 0.008	Not correlated
	Ghose-Crippen octanol-water partition coeff. (logP) (ALOGP)	r = 0.662, p = 0.007	r = 0.671, p = 0.006	Not correlated
	squared Ghose-Crippen octanol-water partition coeff. (logP^2) (ALOGP)	r = 0.712, p = 0.003	r = 0.662, p = 0.007	Not correlated

	surface area of acceptor atoms from P_VSA-like descriptors (SAacc)	r = -0.559, p = 0.030	r = -0.694, p = 0.004	Not correlated

[a] n = total number of molecular descriptors/block included in the study; these molecular descriptors were given by Dragon 7.0 software, excepted the % of cationic form at pH = 7.4 for the block "Charges descriptors", which was determined using Chemicalize software.

Highlights

- Various HAAs inhibit activity of the organic cation transporters OCT1, OCT2 and OCT3
- Trp-P-1 and Trp-P-2 are ones of the most active HAAs against OCT activities
- HAA IC_{50} towards OCTs are higher than expected HAA concentrations in humans
- Trp-P-1 and Trp-P-2 are not substrates for OCT1 and OCT2

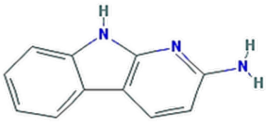

AαC

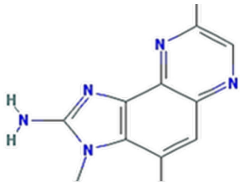

4.8-diMeIQx

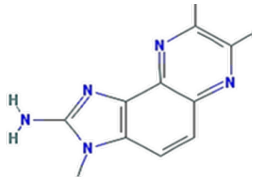

7.8-diMeIQx

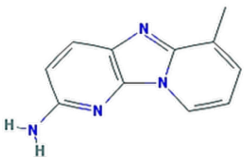

Glu-P-1

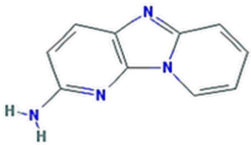

Glu-P-2

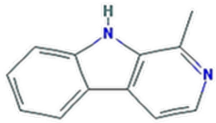

Harmane

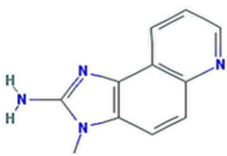

IQ

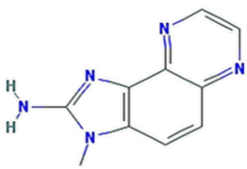

IQx

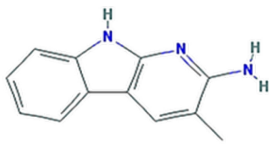

MeAαC

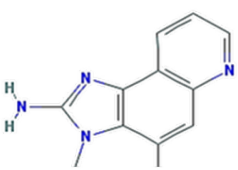

MeIQ

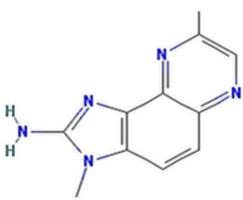

MeIQx

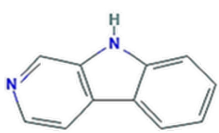

Norharmane

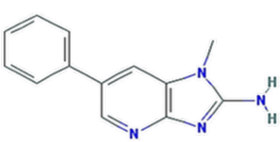

PhIP

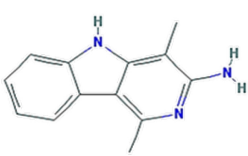

Trp-P-1

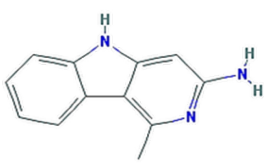

Trp-P-2

Figure 1

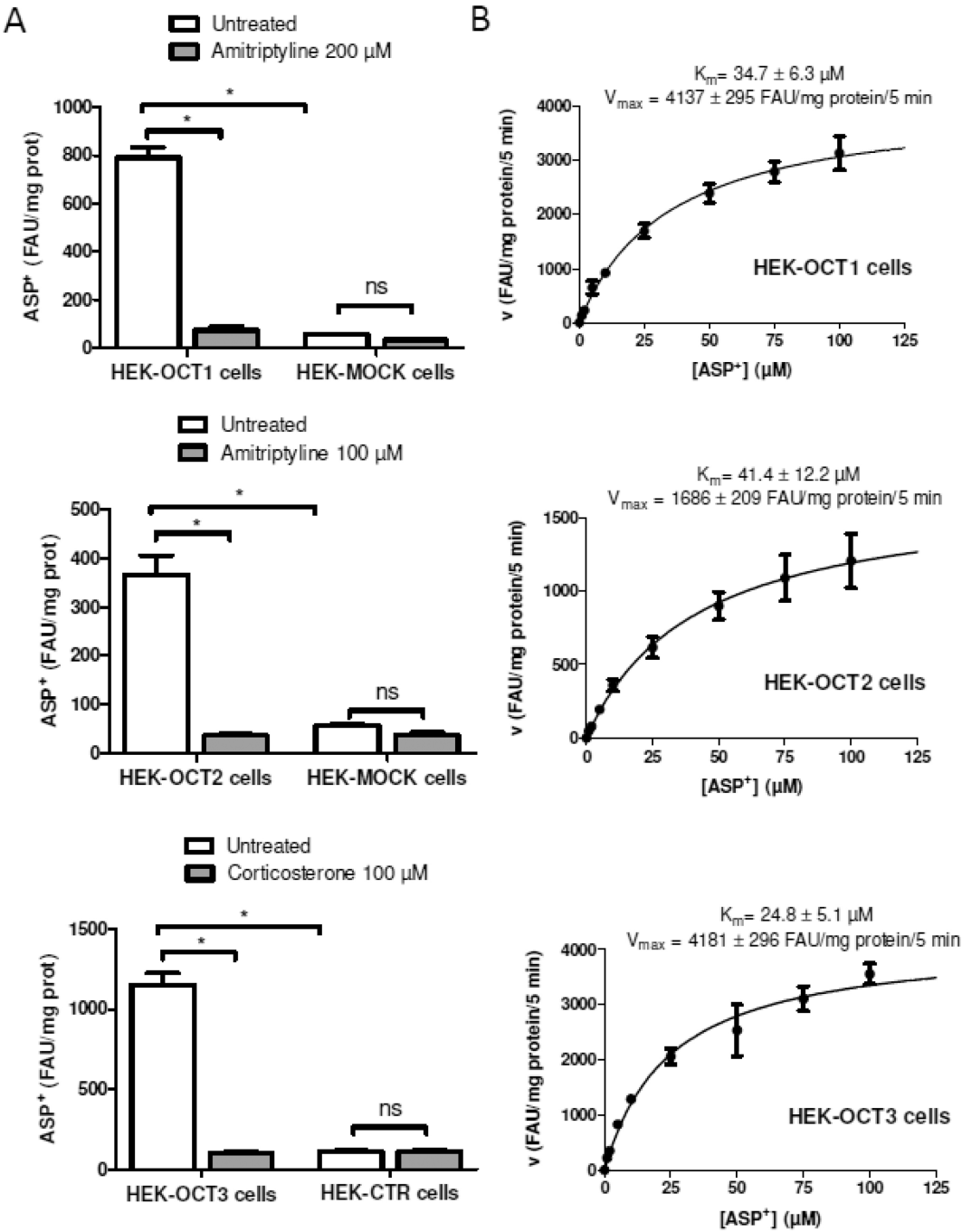
A
Untreated
Amitriptyline 200 µM
ASP+ (FAU/mg prot)
1000
800
600
400
200
0
*
*
ns
HEK-OCT1 cells
HEK-MOCK cells
B
Km= 34.7 ± 6.3 µM
Vmax = 4137 ± 295 FAU/mg protein/5 min
v (FAU/mg protein/5 min)
4000
3000
2000
1000
0
HEK-OCT1 cells
0
25
50
75
100
125
[ASP+] (µM)
Untreated
Amitriptyline 100 µM
ASP+ (FAU/mg prot)
500
400
300
200
100
0
*
*
ns
HEK-OCT2 cells
HEK-MOCK cells
Km= 41.4 ± 12.2 µM
Vmax = 1686 ± 209 FAU/mg protein/5 min
v (FAU/mg protein/5 min)
1500
1000
500
0
HEK-OCT2 cells
0
25
50
75
100
125
[ASP+] (µM)
Untreated
Corticosterone 100 µM
ASP+ (FAU/mg prot)
1500
1000
500
0
*
*
ns
HEK-OCT3 cells
HEK-CTR cells
Km= 24.8 ± 5.1 µM
Vmax = 4181 ± 296 FAU/mg protein/5 min
v (FAU/mg protein/5 min)
4000
3000
2000
1000
0
HEK-OCT3 cells
0
25
50
75
100
125
[ASP+] (µM)

Figure 2

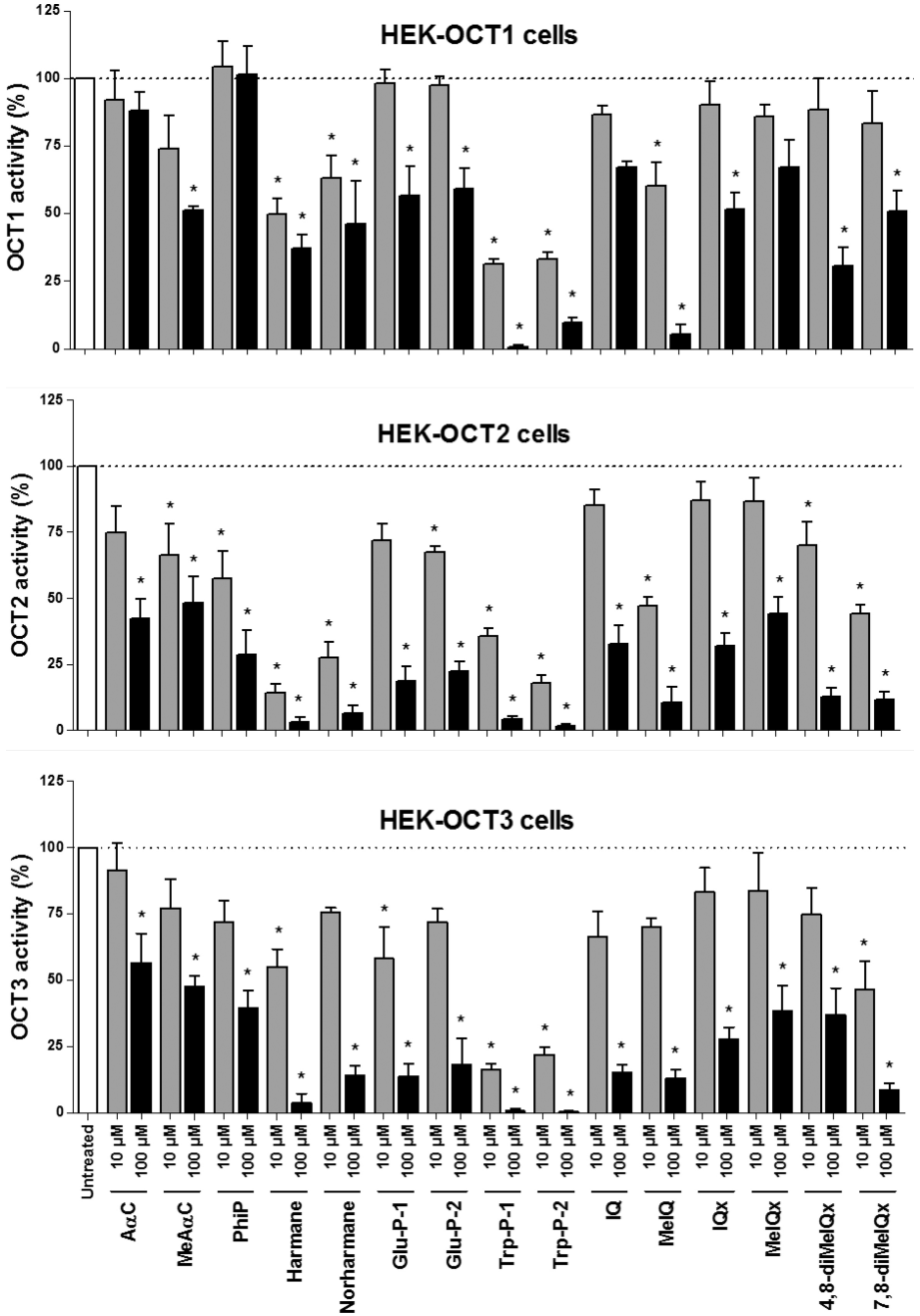
HEK-OCT1 cells
OCT1 activity (%)
HEK-OCT2 cells
OCT2 activity (%)
HEK-OCT3 cells
OCT3 activity (%)
125
100
75
50
25
0
Untreated
10 µM
100 µM
AαC
MeAαC
PhiP
Harmane
Norharmane
Glu-P-1
Glu-P-2
Trp-P-1
Trp-P-2
IQ
MeIQ
IQx
MeIQx
4,8-diMeIQx
7,8-diMeIQx

Figure 3

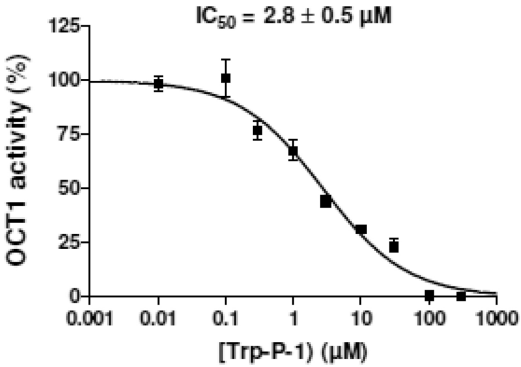
IC50 = 2.8 ± 0.5 µM
OCT1 activity (%)
125
100
75
50
25
0
0.001
0.01
0.1
1
10
100
1000
[Trp-P-1) (µM)

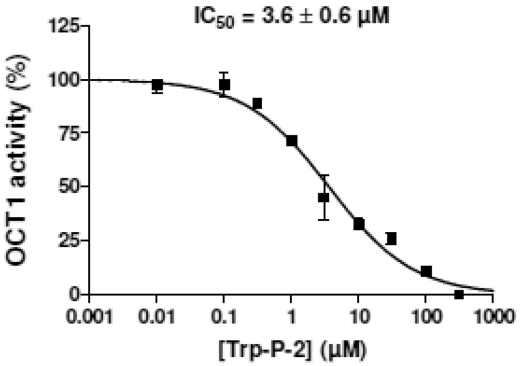
IC50 = 3.6 ± 0.6 µM
OCT1 activity (%)
125
100
75
50
25
0
0.001
0.01
0.1
1
10
100
1000
[Trp-P-2] (µM)

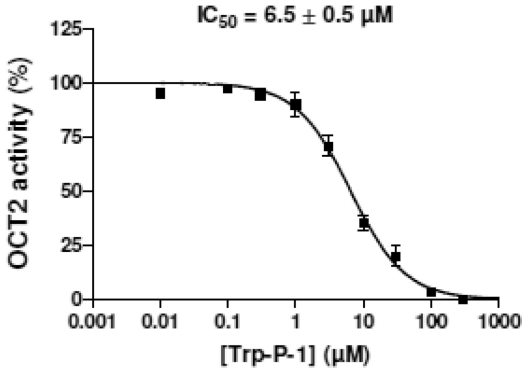
IC50 = 6.5 ± 0.5 µM
OCT2 activity (%)
125
100
75
50
25
0
0.001
0.01
0.1
1
10
100
1000
[Trp-P-1] (µM)

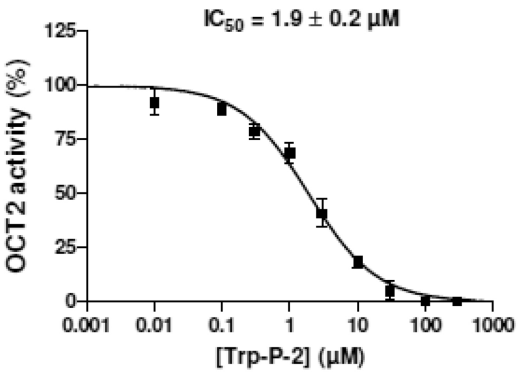
IC50 = 1.9 ± 0.2 µM
OCT2 activity (%)
125
100
75
50
25
0
0.001
0.01
0.1
1
10
100
1000
[Trp-P-2] (µM)

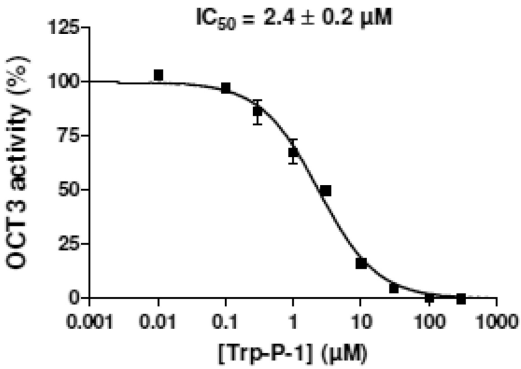
IC50 = 2.4 ± 0.2 µM
OCT3 activity (%)
125
100
75
50
25
0
0.001
0.01
0.1
1
10
100
1000
[Trp-P-1] (µM)

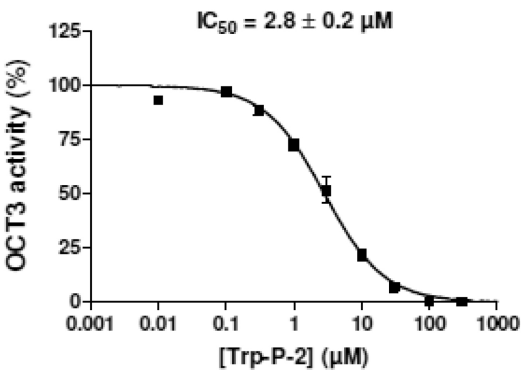
IC50 = 2.8 ± 0.2 µM
OCT3 activity (%)
125
100
75
50
25
0
0.001
0.01
0.1
1
10
100
1000
[Trp-P-2] (µM)

Figure 4

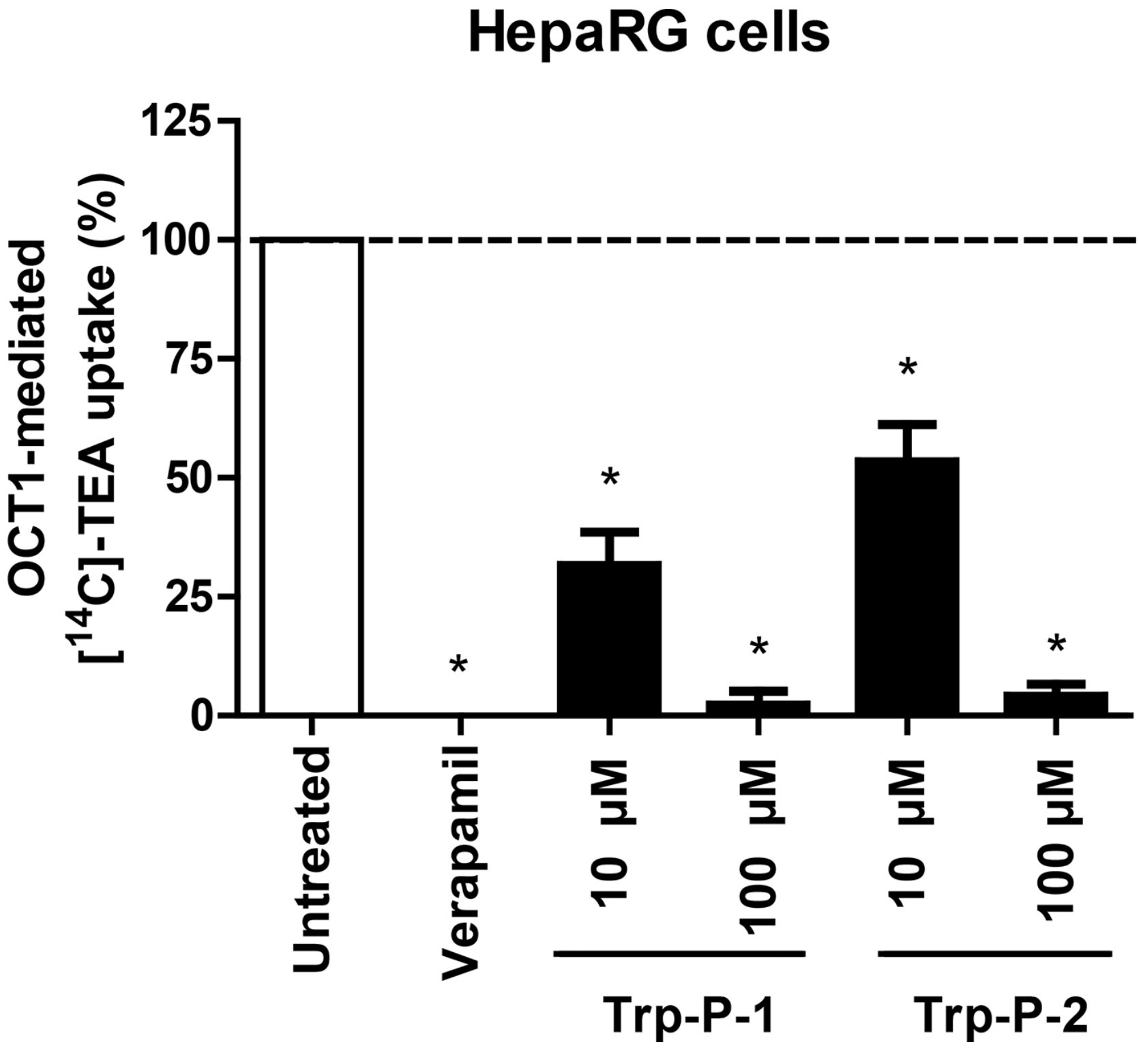
HepaRG cells
OCT1-mediated
[14C]-TEA uptake (%)
125
100
75
50
25
0
*
*
*
*
*
Untreated
Verapamil
10 µM
100 µM
10 µM
100 µM
Trp-P-1
Trp-P-2

Figure 5

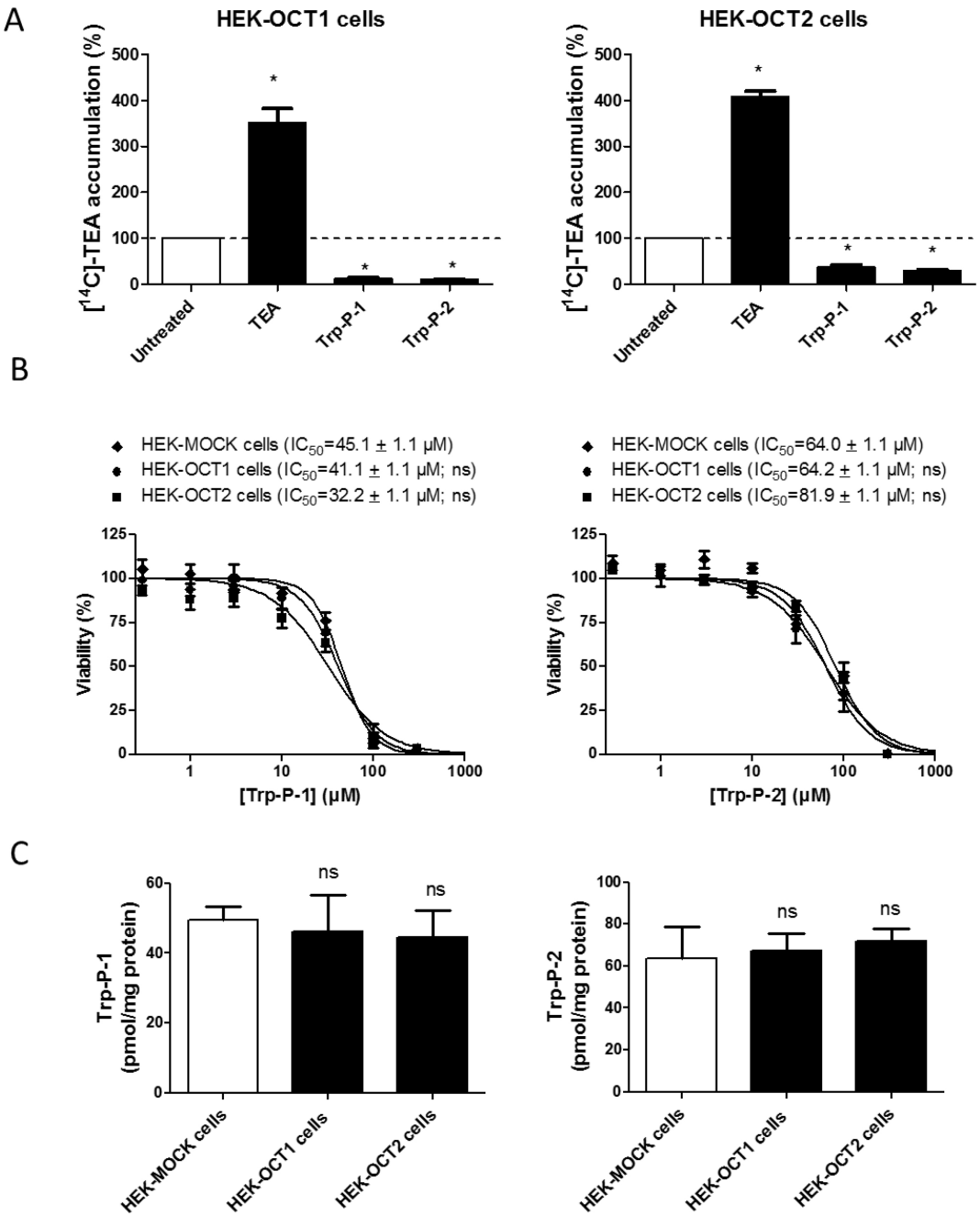
A
HEK-OCT1 cells
HEK-OCT2 cells
[14C]-TEA accumulation (%)
500
400
300
200
100
0
*
Untreated
TEA
Trp-P-1
Trp-P-2
B
HEK-MOCK cells (IC50=45.1 ± 1.1 μM)
HEK-OCT1 cells (IC50=41.1 ± 1.1 μM; ns)
HEK-OCT2 cells (IC50=32.2 ± 1.1 μM; ns)
HEK-MOCK cells (IC50=64.0 ± 1.1 μM)
HEK-OCT1 cells (IC50=64.2 ± 1.1 μM; ns)
HEK-OCT2 cells (IC50=81.9 ± 1.1 μM; ns)
Viability (%)
125
100
75
50
25
0
1
10
100
1000
[Trp-P-1] (μM)
[Trp-P-2] (μM)
C
Trp-P-1 (pmol/mg protein)
Trp-P-2 (pmol/mg protein)
60
40
20
0
80
ns
HEK-MOCK cells
HEK-OCT1 cells
HEK-OCT2 cells

Figure 6

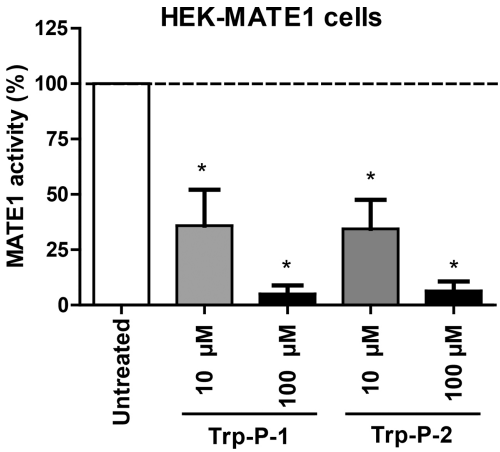
HEK-MATE1 cells
MATE1 activity (%)
125
100
75
50
25
0
Untreated
10 µM
100 µM
10 µM
100 µM
Trp-P-1
Trp-P-2

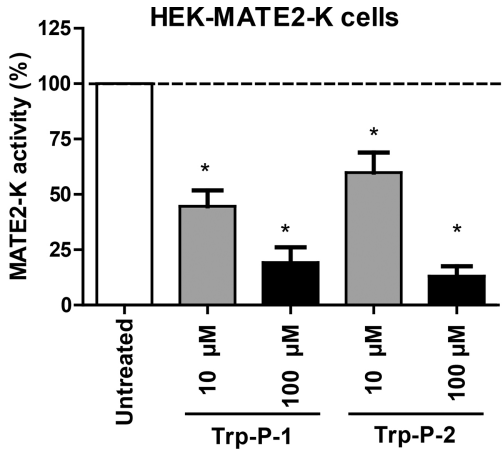
HEK-MATE2-K cells
MATE2-K activity (%)
125
100
75
50
25
0
Untreated
10 µM
100 µM
10 µM
100 µM
Trp-P-1
Trp-P-2

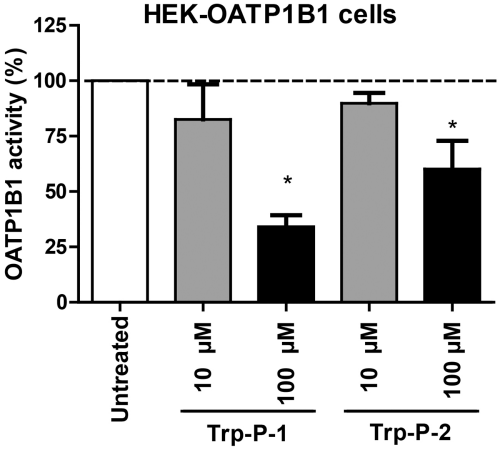
HEK-OATP1B1 cells
OATP1B1 activity (%)
125
100
75
50
25
0
Untreated
10 µM
100 µM
10 µM
100 µM
Trp-P-1
Trp-P-2

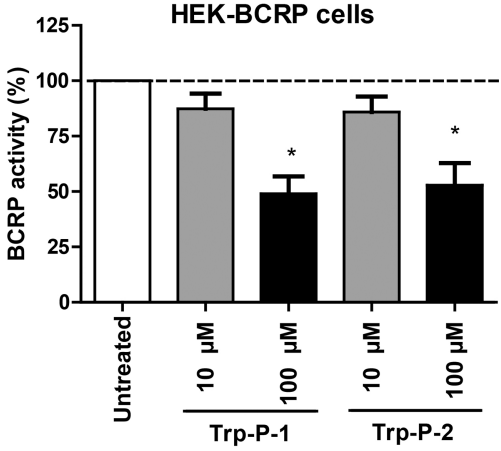
HEK-BCRP cells
BCRP activity (%)
125
100
75
50
25
0
Untreated
10 µM
100 µM
10 µM
100 µM
Trp-P-1
Trp-P-2

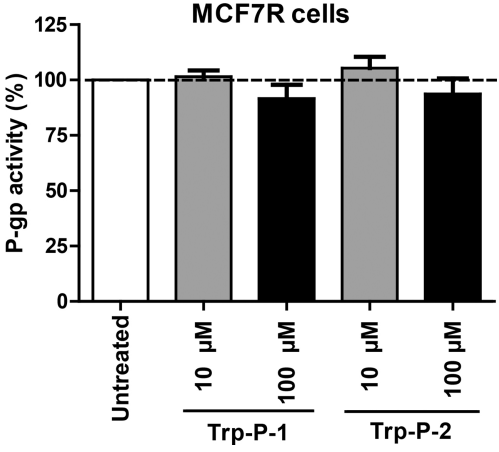
MCF7R cells
P-gp activity (%)
125
100
75
50
25
0
Untreated
10 µM
100 µM
10 µM
100 µM
Trp-P-1
Trp-P-2

Figure 7